ISSN: 2319-5967
ISO 9001:2008 Certified
International Journal of Engineering Science and Innovative Technology (IJESIT)
Volume 3, Issue 3, May 2014

High ionic conduction in nanocrystalline ytterbium stabilized zirconia grown by ultrasonic spray pyrolysis

Adriana Benítez-Rico[1], Mario F. García Sánchez[2], Betsabée M. Monroy-Pelaez[1], Jaime Santoyo-Salazar[3], M. López-López, Guillermo Santana-Rodríguez[1,3*].

[1] Instituto de Investigaciones en Materiales, Universidad Nacional Autónoma de México. A.P. 70-360, Coyoacán, C.P. 04510, México, D.F.

[2] Unidad Profesional Interdisciplinaria en Ingeniería y Tecnologías Avanzadas. Instituto Politécnico Nacional, Av. I.P.N. 2580, Gustavo A. Madero, 07340, México .D.F.

[3] Departamento de Física, CINVESTAV-IPN, A.P. 14-740, C.P. 07000, México, D.F.

Abstract*— Nanocrystalline thin films of ytterbium stabilized zirconia (YbSZ) have been grown on single-crystalline silicon substrates by ultrasonic spray pyrolysis using ytterbium acetate and zirconium acetylacetonate as metallo-organic precursors dissolved in anhydrous methanol. The morphology, structure and electrical properties were studied by atomic force microscopy (AFM), scanning electron microscopy (SEM), X-ray diffraction (XRD), transmission electron microscopy (TEM) and impedance spectroscopy (IS). The precursor solution and the spray conditions were optimized for obtaining smooth, dense and homogeneous nanocrystalline films with grains sizes smaller than 10 nm. The cubic phase was considered to make the XRD analyses of the spectra as this phase is more stable in these types of materials. The activation energy in grains is similar to the reported values in YbSZ, and increases with the increase of ytterbium content. On the other side, activation energy of the grain boundaries decreases with the increase of ytterbium content. These activation energy values are related to the small grain sizes and the close boundaries obtained at the optimized conditions. A high conductivity of the order of 0.64 S/m at 400 ºC was obtained for 4% of ytterbium.

***Index Terms*— Ionic conduction, ultrasonic spray pyrolysis, XRD, YbSZ.**

I. INTRODUCTION

In recent years, nanoscale structures were shown as means for potentially increasing the transport properties in oxides of relevance to solid oxide fuel cells (SOFC) and sensors [1,2]. These results will allow a meaningful decrease of the operation temperature of these devices to the intermediate range (500-700ºC) and increase its competitiveness. The causes of this enhancement in the conductivity are not yet understood and there are still many scientific interests in the analysis of this phenomenon [3-6] . Yttrium stabilized zirconia (YSZ) has long been used as the electrolyte of choice in solid oxide fuel cells [1]. During the last years, considerable attention has been focused on the deposition of smooth, homogeneous and dense thin films of YSZ [7-15]. Recently, enhanced conductivity of nanostructured YSZ thin films has been reported [16-18]. There are other rare earth dopants that can be used to stabilize zirconia with better electrical performance, in particular Sc and Yb and some papers report the electrical performance in nanocrystalline scandium stabilized zirconia [19, 20]. To our knowledge there are no reports in nanocrystalline ytterbium stabilized zirconia (YbSZ). Among thin film deposition techniques, ultrasonic spray pyrolysis offers the possibility to produce nanostructured and dense thin films of different materials at atmospheric pressure [21,22]. The deposition temperature, flow rates and initial droplet size are the main parameters controlling film properties. Recently, nanocrystalline microstructures of YSZ and CeO_2 with grain sizes lower than 10 nm have been reported using ultrasonic spray pyrolysis deposition [18,23].

In this work, ultrasonic spray pyrolysis was used to grow YbSZ thin films with nanometric grain size. The influence of different deposition parameters in the structural and electrical properties for different chemical compositions are discussed and compared with previous reports.

ISSN: 2319-5967
ISO 9001:2008 Certified
International Journal of Engineering Science and Innovative Technology (IJESIT)
Volume 3, Issue 3, May 2014

II. EXPERIMENTAL PROCEDURE

The experimental setup shown in García Sánchez et al. [18] was used. The diameter of the nozzle was 16 mm and the distance nozzle-substrate was fixed to 20 mm. Films were deposited onto (100) n-type, 200 Ω-cm single crystalline silicon slices. The substrates were ultrasonically cleaned with trichloroethylene, acetone and methanol for surface removal of dirt and degreasing. Also, etching with 5% HF solution was used in order to remove the Si native oxide. The precursor solution was prepared by dissolving calculated mixtures of zirconium (IV) acetylacetonate [$Zr(acac)_4$=$Zr(C_5H_7O_2)_4$] 98% and ytterbium acetate tetrahydrate [$Yb(ac)_3 \cdot 4H_2O$] 99.9% from Sigma-Aldrich Chemicals in anhydrous methanol (Fischer 99.9%). These salts were chosen as precursors of YbSZ films with different ytterbium/zirconium molar ratios (between 0.04 and 0.12 mol percent). 1 ml of acetic acid (CH_3COOH) was added for each 0.5 l of anhydrous methanol. The precursor solution was nebulized in a custom-made spray setup based on a commercially available ultrasonic nebulizer (YUE HUA WH-802) operating at a frequency of 107 MHz. The carrier gas flow rate was fixed at 1.5 l/min and directing gas (air in both cases) was varied between 1.5 and 3.5 l/min. The substrate temperature (T_s) was controlled in the range of 300-550ºC, and the deposition time (t_d) was varied between 5 and 25 min. Surface morphology and energy dispersive X-ray (EDS) analyses were performed with a field-emission scanning electron microscope JEOL-7600F at 15 kV. An atomic force microscope (Jeol JSPM-4210) in tapping mode with high resolution tips (MikroMasch DP15/HI'RES/AIBS/15) under normal pressure conditions was employed to evaluate the surface of the films. X-ray diffraction patterns were obtained with a Rigaku DMAX 2200 equipment using the CuKα wavelength, the XRD spectra were obtained for theta angles from 2° to 70° with steps 0f 0.020º. The unit cell parameters were calculated using the Celref3 program. TEM specimens with a thickness around 100 nm were prepared using a fine energetic beam of gallium ions (JEOL JEM-9329FIB). Particle size, nanoparticle distribution and electron diffraction patterns were determined by transmission electron microscopy TEM using a JEOL JEM2010 operating at 200 kV. The thickness of the films was measured with a profilometer by contact stylus method (VeecoDektak 150). For this purpose, a small part of the substrate was covered with one little piece of Pyrex glass to form a step during deposition. The thickness of film was also measured by null ellipsometry (Gaertner 117A ellipsometer) using the 632.8 nm line from a He-Ne laser. Both methods, ellipsometry and profilometry, gave similar thickness values for films deposited at the same conditions. The room-temperature refractive index was calculated using the GEMP^{TM} software provided by the ellipsometer. AC conductivity was measured using a frequency–response analyzer (SOLARTRON SI 1260 with dielectric interface) in the frequency range 0.01Hz-10MHz to investigate the electrical properties for temperatures between 100-450°C. A parallel pattern of two platinum electrodes was sputtered on the film surface. Impedance diagrams were fitted by equivalent circuit method.

III. RESULTS AND DISCUSSION

(1) Influence of solution.

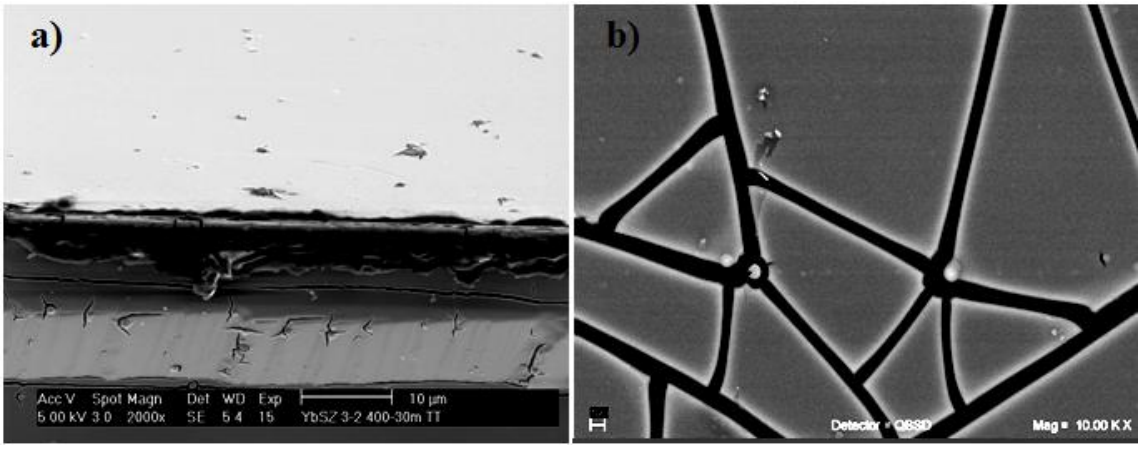

Fig. 1. SEM images of YbSZ films grown at 450 ºC and 0.025 M solution: a) cross section of a grown film and b) sample with thermal annealing at 600 ºC for 2 h.

ISSN: 2319-5967
ISO 9001:2008 Certified
International Journal of Engineering Science and Innovative Technology (IJESIT)
Volume 3, Issue 3, May 2014

First, samples were grown with a 0.025 M solution at temperatures between 300 and 500 ºC, according to previous results obtained for YSZ [18] with flow rates of 1.5 l/min for both, directing and carrier gas. All films presented particles in the surface. Figure 1a shows a SEM cross section image where it can be observed that microscopic particles are distributed inside the film. These particles produce severe cracks when a thermal annealing was conducted onto the films (figure 1b). This effect was associated to undissolved precursors in solution. To allow the complete solubility of precursors, solution molarity was reduced to 0.01 M. Additionally, in concordance to previous results, acetic acid was added to avoid the formation of hydroxides in solution [23,24].

(2) Optimization of films growth conditions.

Film quality is influenced by several parameters. The decrease of solution molarity also decreases the deposition rate of films, which is not desired. Once a stable solution was obtained, directing gas flow rates were increased to 3.5 l/min searching to not greatly affect the deposition rate. Higher flow rates avoid the formation of a constant mist. Unlike those reported in CeO_2 [23], splashes were not observed in any films, maybe due to the low precursor molarity in the solution. As CVD conditions were desired, this increase in the flow rate required increasing the substrate temperature. TGA analysis shows that the decomposition temperature of precursors was around 400 ºC, therefore, substrates temperature were varied from 400 ºC to 550 ºC. Finally, the optimal conditions to obtain dense, smooth and crack free films which are shown in figures 2a and 2b, were: solution precursor concentration, 0.01 M and pH ~ 4; substrate temperature, 550 °C; deposition time, 20 minutes. In figure 2b it can be observed that smooth and crack free films are obtained, even with a thermal annealing at 700 °C for 2 h.

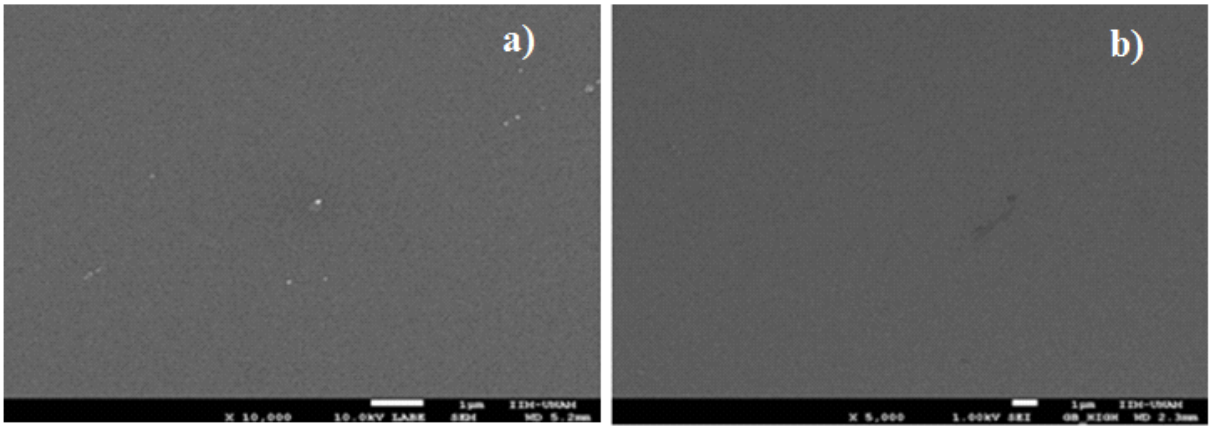

Fig. 2. SEM images of YbSZ films grown at 550 ºC and 0.01 M solution: a) as grown and b) with thermal annealing at 700ºC for 2 h.

(3) Influence of composition

Once experimental growth conditions were established, YbSZ thin films with Yb mol percents 4, 6, 8, 10 and 12% were grown. Figure 3 shows the relative concentrations of ytterbium with respect to zirconium obtained by EDS. This analysis shows that Zr and Yb in the film were almost in the same proportion as in the precursor solution. Chemical homogeneity of samples was also verified scanning different zones by EDS.

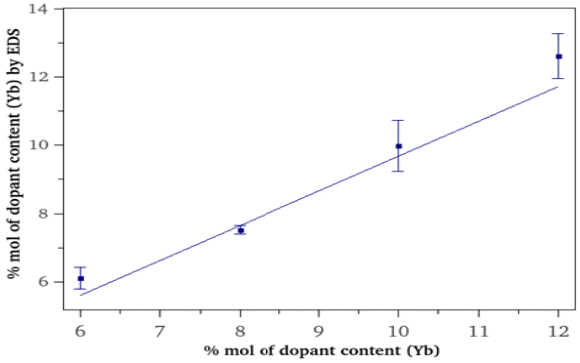

Fig. 3.Yb to Zr ratios obtained by EDS.

ISSN: 2319-5967
ISO 9001:2008 Certified
International Journal of Engineering Science and Innovative Technology (IJESIT)
Volume 3, Issue 3, May 2014

Figure 4a shows typical XRD patterns for the as grown films with different ytterbium contents. In this figure the presence of four main peaks can be observed which are associated to the cubic phase of YbSZ (JCPDS file No. 027-0997) with a fluorite structure (space group *Fm3m*). Other peaks with low intensity can be observed at lower concentrations of Yb (4-8%), which can be associated to a monoclinic phase (JCPDS file No. 013-0307). The two phase region (monoclinic + cubic) has been previously reported by Hartmanová et al. at low Yb molarity using a Rietveld analysis of the XRD data [25,26]. They report that the monoclinic phase is reduced with the increase of molarity, which is in concordance to the present results. A tetragonal phase has also been reported in nanometric zirconia thin films or for low ytterbium concentration [19,27], but the peaks corresponding to these phases are overlapped and it is very difficult to differentiate them. The cubic phase was considered to make the analyses of the XRD spectra as this phase is more stable in these materials [18]. In general, reflections could be indexed by the cubic or tetragonal structure due to the combined actions of the crystallite size effect and the existence of adequate stabilizers (Yb^{3+} ions). Additionally, no extra peaks associated with ytterbia and m-ZrO_2 were observed in these samples. In the considered phase, Yb^{3+} ions replace Zr^{4+} ions in the structure creating O^{2-} vacancies (figure 4b), which allows the ionic conduction (figure 4c).

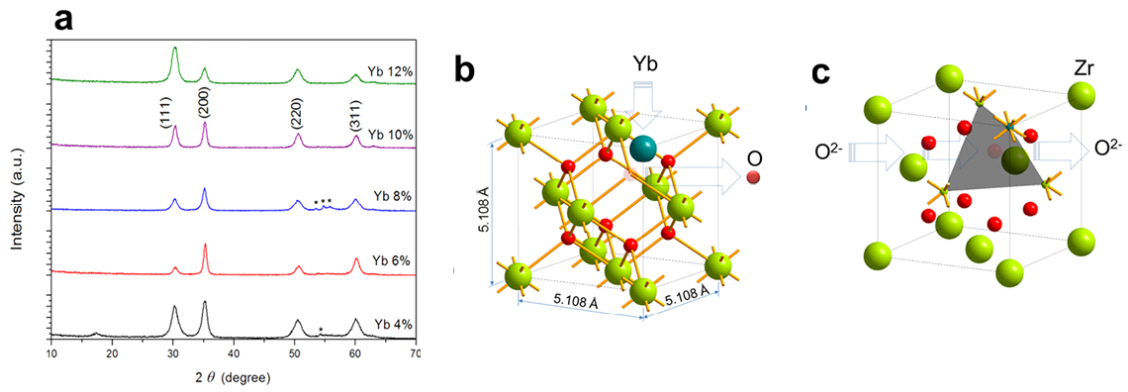

Fig 4. a) XRD pattern of deposited samples. b) Yb added to ZrO_2 cubic structure FCC and O vacancies. c) Indicates the ionic conductivity through O vacancies in tetrahedral positions.

Lattice parameters (a) calculated from the XRD peak positions are presented in Table I. Lattice parameters reported in reference [28] increase with Yb concentration. However, no major changes were observed in this parameter within the margin of error of our experiments, unlike those reported by Harmanová et.al. [26]. This could be a consequence of the low resolution of the difractogram or the small grain sizes obtained in our case.The average crystallite sizes (D) were estimated from XRD patterns for the (200) peak, using the Scherrer formula corrected for the instrument contribution, as:

$$D = \frac{0.9\lambda}{\beta \cos\Theta_B} \qquad (1)$$

Here, λ is the wavelength of the incident beam, β is the intrinsic width at half maximum of the *hkl* line and Θ_B is the Bragg diffraction angle. Average crystallite sizes less than 11 nm were obtained in all cases, which are reported in table I. The nanometric crystallite size can be associated to the low precursor solution concentration and the ultrasonic generated aerosol [18].

Table I. Optical and structural parameters of prepared samples.

Ytterbium (%)	Lattice parameter (Å)	Grain size (nm)	RMS roughness (nm)	Refractive index	Relative density
4	5.10 ± 0.03	6.6	1.00±0.20	2.00 ± 0.02	0.92
6	5.09 ± 0.02	9.7	1.15 ±0.18	2.04 ± 0.01	0.94
8	5.10 ± 0.03	5.3	1.00 ±0.10	1.96 ± 0.04	0.90
10	5.10± 0.02	10.6	1.30 ±0.13	2.01 ± 0.04	0.93
12	5.11± 0.02	6.9	1.01 ±0.2	1.89 ± 0.01	0.85

ISSN: 2319-5967
ISO 9001:2008 Certified
International Journal of Engineering Science and Innovative Technology (IJESIT)
Volume 3, Issue 3, May 2014

Figure 5 shows a TEM cross section of film YbSZ-10%. It can be observed that samples are homogeneous throughout all the film's thickness (figure 5a), where the particle size is lower than 10 nm, in correspondence with the particle size calculated previously. TEM analysis shows the interatomic distances corresponding to the cubic structure in the nanoparticles at [200], (figure 5b and 5c). Selected Area Electron Diffraction, SAED is characterized by diffracted rings from nanoparticles distributed along the film. The distance between these rings corresponds to interatomic distances and crystalline planes of cubic phase YbSZ. The description of the structure is compared with calculated values in XRD (figure 5d) and these have the same structural correspondence.

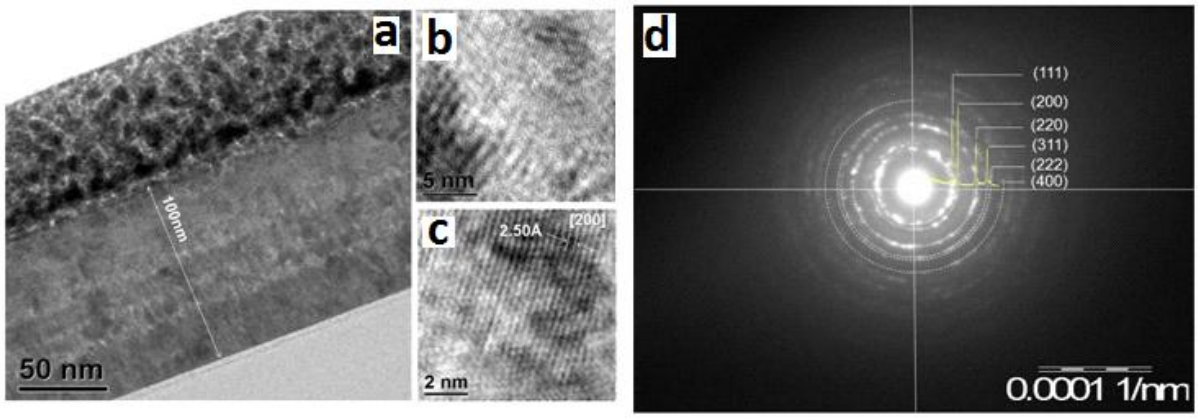

Fig. 5. TEM image of YbSZ-10% thin films.

A very important result to be noticed is the stress due to the defect states in the surfaces of grains observed in the films directly by TEM (figure 6a). Some lines formed across the thin film are identified as the contribution of high concentration of defects. The defects follow their path over the grain and grain boundaries, and these form small blocks along the thin films (figure 6b). This stress has been recently associated to the high ionic conductivity reported in these nanostructured materials [3-6]. The stress is likely due to the changes in lattice parameters and grain sizes aroused by the Yb^{3+} doping effect.

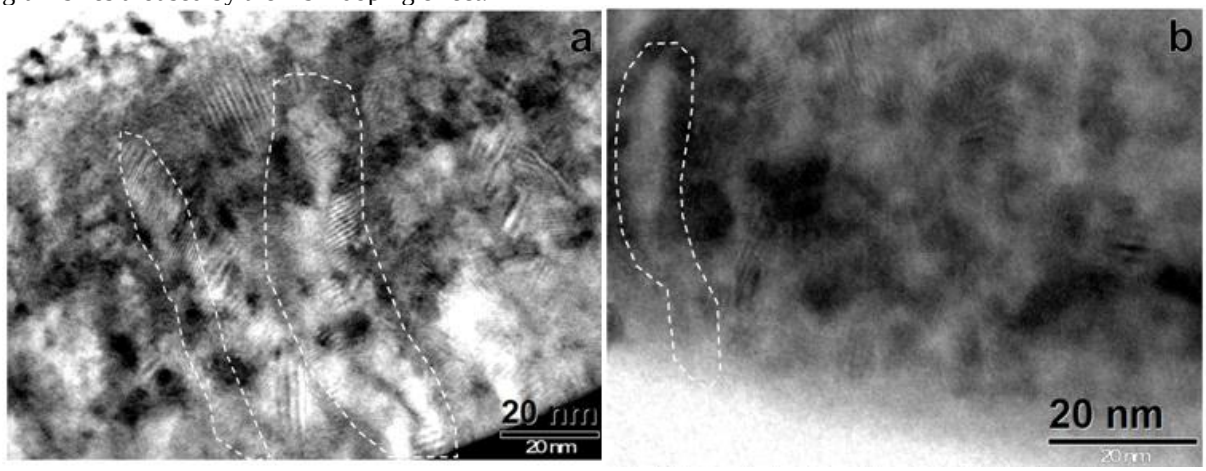

Fig. 6. TEM images where the stress in the film can be observed in the middle of dashed areas.

Figure 7 shows the variation of film thickness with deposition time for YbSZ-10% at 550 °C. The film thickness increases linearly with deposition time. The film deposition rate is 23 nm/min, which is similar to previous reports in films grown by this technique at higher molarities [18,23]. This is a consequence of increasing the directing gas flow rate and the deposition temperature. Similar results were obtained for the other Yb compositions.

ISSN: 2319-5967
ISO 9001:2008 Certified
International Journal of Engineering Science and Innovative Technology (IJESIT)
Volume 3, Issue 3, May 2014

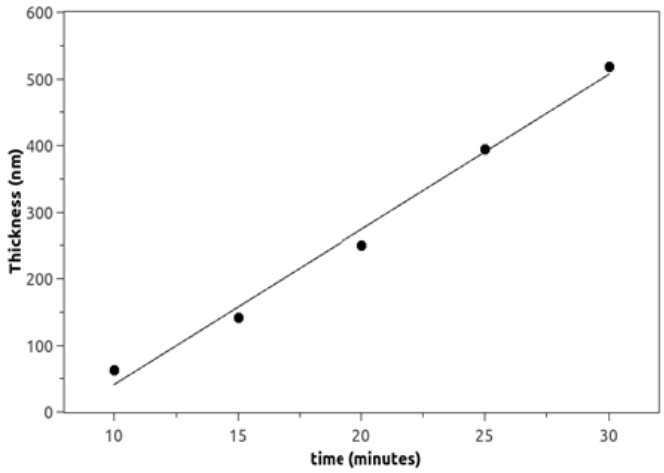

Fig. 7. Growth rate for YbSZ-10% at 550°C, calculated from slope ~ 23 nm/s.

Figure 8a shows AFM morphology of YbSZ-8% film. A smooth and homogeneous surface can be observed. Table I reports the RMS roughness values calculated for all prepared compositions. A RMS roughness of around 1 nm was obtained in all cases. When composition of Yb is incremented to 12% (figure 8b), the surface is more irregular, while the roughness is maintained. Surface clusters of around 23 nm are observed, but these seem to consist of smaller grains. Similar results were observed in the other compositions.

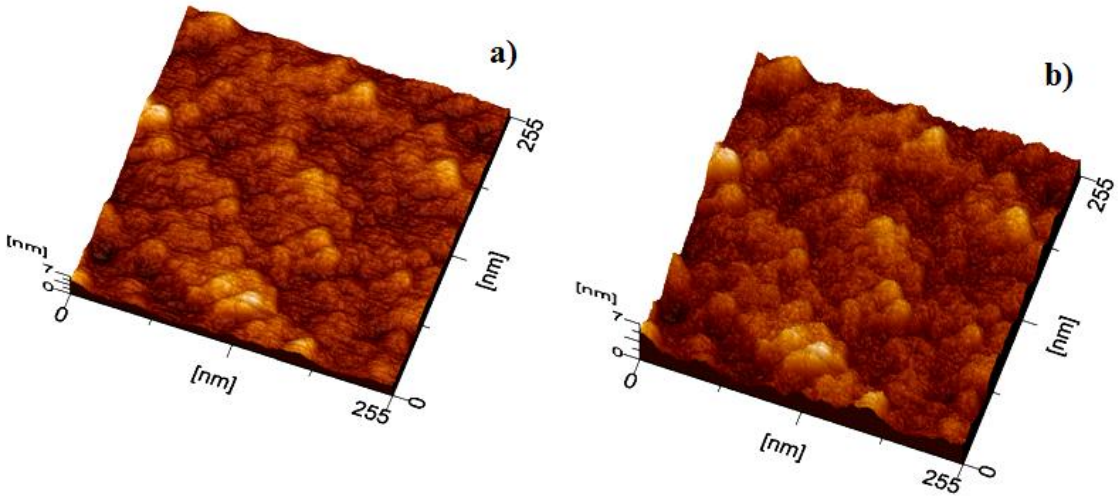

Fig. 8. Atomic force microscopy images of films with a) 8% and b) 12% mol of Yb.

Figure 9 shows the refractive index values for films prepared in this work. Values reported by Hartridge et.al. are presented in the same graph for comparison [28]. Refractive index values around 2 are obtained for all compositions, excepting YbSZ-12%. Refractive index of ZrO_2 with cubic structure is around 2.1-2.2. Porosity decreases the refractive index of films, which indicates a lower density for the 12% composition. In any case, the expected density of our samples is higher than reported by Hartridge et. al in thin films grown by dipping of a solution and then annealed at 1050 °C. Table I reports the relative density obtained using the Lorentz-Lorentz law to relate the film density with refractive index [29]. The high homogeneity and density of the films have been associated to the use of an ultrasonic mist and lower molarity of precursors in the solution, which permitted to obtain small droplets in the mist with homogeneous ratios [18].

ISSN: 2319-5967
ISO 9001:2008 Certified
International Journal of Engineering Science and Innovative Technology (IJESIT)
Volume 3, Issue 3, May 2014

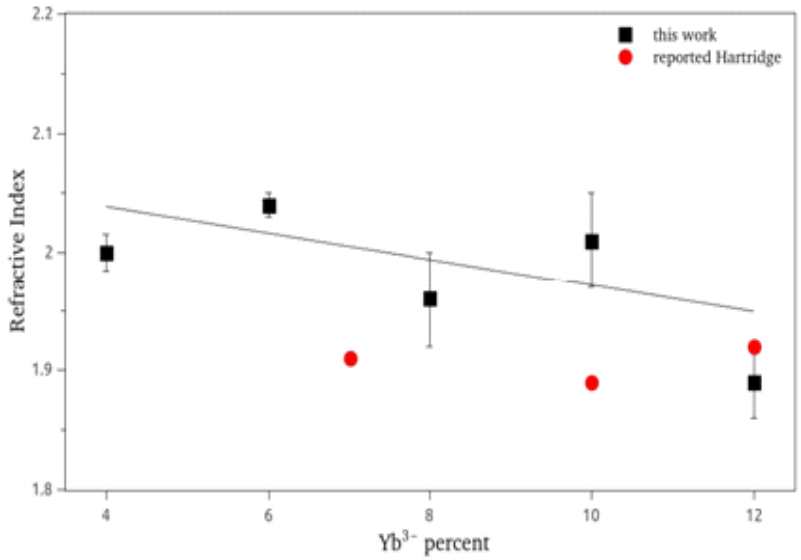

Fig. 9. Refractive index vs. Yb content.

(4) Electrical properties.

Figure 10 shows a representative impedance complex plane plot of sample YbSZ-8% measured at 300 °C. Two overlapping and slightly compressed semicircles were observed in the impedance complex plane plot. This behavior is indicative of two processes and it was associated with the electrolyte bulk (grain) and the grain boundary, in correspondence with previous reports [18, 27]. The impedance diagrams were simulated, using the Zview program, by a series network of two sub-circuits, each one consisting of one resistor and one Constant Phase Element (CPE) in parallel. The CPE is incorporated for adjusting the depression below the baseline of semicircles, typical in ionic conductors [30-33]. From this simulation the total resistance, *R*, was determined for each impedance diagram from the interceptions of the observed semicircle on the real axis of the impedance spectra and then the conductivity of each film as a function of temperature was calculated from the expression $\sigma=K/R$, where *K* is the geometric factor. The contribution of the Si substrate to the total resistance can be neglected because it is various orders of magnitude lower. A maximum value of total conductivity at 400 ºC, 0.64 S/cm, was obtained for films with 4% of ytterbium. The low value of conductivity can be associated with the decrease of activation energy, the high density of samples, or maybe the stress in the nanostructures. More studies are necessary to understand the relationship between the nanoparticles sizes and the conductivity in these materials.

The plot of log (σT) versus 1/T adjust quite well to straight lines (not shown), which indicates that the conductivity for all these samples can be expressed in the form of the Arrhenius relationship: $\sigma T=A \exp(-E_a/kT)$, where E_a is the activation energy for ion migration, A is the pre-exponential factor, k is the Boltzman constant and T is the temperature in Kelvin.

The activation energy of grains (figure 11) is slightly lower than the reported values in bulk for this material [27,28]. We expected to obtain similar values as the activation energy is an intrinsic parameter of the material and it is not supposed to change with the way of preparation of the material [18]. The differences may be associated to the stress in the nanometric grains [4,5]. The dependence of E_a on the Yb^{3+} doping concentration observed in this study could be explained by the energy variations involved in the ion-transport behavior. Generally, the grains E_a is the sum of the migration energy for oxide anions migrating through the zirconia lattice and the binding energy between oxygen vacancies and doping cations. At low Yb^{3+} doping concentration, the migration energy is the dominant term, which comprises the energy required to break a lattice cations-oxygen bond and an energy term dependent on oxide ion mobility between vacancies. When the doping is increased slowly the activation energy is increased too due to the fact that the Yb-O bond is stronger than the Zr-O bond [34]. Under this condition, considering that the effect of the energy term related to the oxide ion mobility between vacancies is slight, an increase in the doping concentration impacts on an increase in E_a. At higher Yb concentration, since the

ISSN: 2319-5967
ISO 9001:2008 Certified
International Journal of Engineering Science and Innovative Technology (IJESIT)
Volume 3, Issue 3, May 2014

concentration of vacancies is increased drastically, the binding energy for Yb cations and vacancies become the dominant term. As a result, the activation energy E_a increases remarkably for 12%. But the activation energy of the grain boundary is lower, even than the values obtained for grains at higher compositions (figure 11). The decrease in the grain boundaries activation energy is in correspondence with previous reports in thin films and it is related to the nanometric grain size [3,6,16-18,25]. The activation energy of bulk increases with the increase of ytterbium in the structure. Similar results were reported by Hartmanová et.al [25,26]. But in our case the grain boundary activation energy decreases when the content of ytterbium increases.

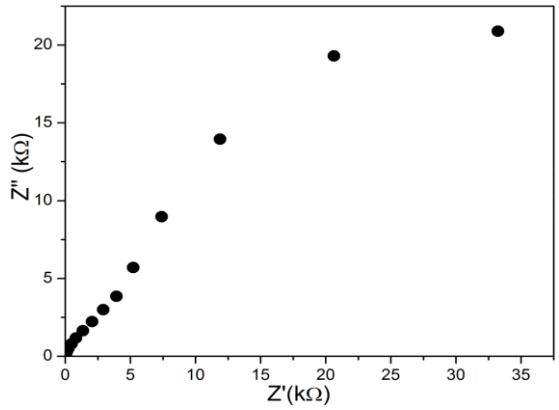

Fig. 10. Representative impedance response measured at 300 °C for the film YbSZ-8%.

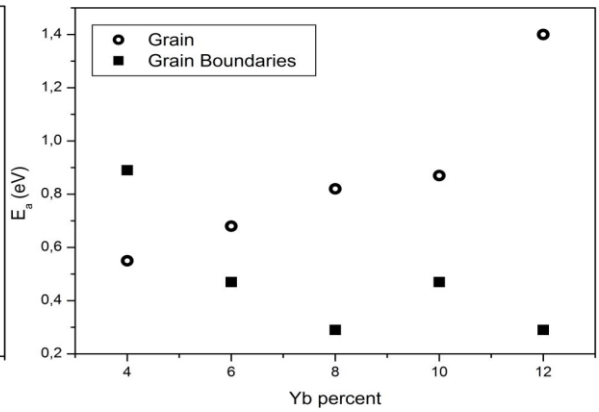

Fig. 11. Activation energy vs. molarity for a) grain and b) grain boundaries

IV. CONCLUSION

Smooth, dense and homogeneous YbSZ films have been deposited in silicon substrates by ultrasonic spray pyrolysis. Acetic acid was added to the solution for obtaining crack free films. The use of ultrasonic generated mist and low concentration of precursor solution permitted to obtain small droplets. The decrease of droplets diameter allowed the use of low substrate temperature, increasing the deposition rate and reducing the splashing residues on the surface. With these experimental conditions nanostructured films with particles sizes smaller than 10 nm were produced. The conductivity of films is increased and the activation energy is reduced with the reduction of porosity and nanoparticles size. Activation energy values in grains increase with the increase of ytterbium content, while the grain boundary has an opposite behavior. This behavior is attributed to the fact that the Yb-O bond is stronger than the Zr-O bond, increasing the binding energy between oxygen vacancies and doping cations. Maximum conductivity was obtained for 4% ytterbium in the films.

ACKNOWLEDGEMENT

The authors acknowledge the technical assistance of Carlos Flores, Josefina Arellano, Omar Novelo and Maria Elena Villafuerte´s Laboratory of IIM-UNAM, Alejandro Esparza of CCADET-UNAM, Patricia Altuzar of IER-UNAM. The authors acknowledge financial support for this work from CONACYT-SENER under contract No.151076 and ICyTDF PICCO 10-29. This work was partially supported by DGAPA-UNAM PAPIIT projects IN102411 and IB101612 and CONACyT México under project 153948. Partial support from IPN with research project 20140321 is gratefully acknowledged.

REFERENCES

[1] Z. Shao, W. Zhou, Z. Zhu, “Advanced synthesis of materials for solid oxide fuel cells”, Prog. Mater. Sci., 57 804 – 874, 2012.

[2] C. López-Gándara, F. M. Ramos, A. Cirera “YSZ-based oxygen sensors and the use of nanomaterials, A review from classical models to current trends”, J. Sens., 258489 (15 pages), 2009.

[3] X. Guo “Can we achieve significantly higher ionic conductivity in nanostructured zirconia?” Scripta Mater., 65 96 – 101, 2011.

ISSN: 2319-5967
ISO 9001:2008 Certified
International Journal of Engineering Science and Innovative Technology (IJESIT)
Volume 3, Issue 3, May 2014

[4] J. L. M. Rupp "Ionic diffusion as a matter of lattice-strain for electro ceramic thin films" Solid State Ionics, 207 1-13, 2012.

[5] A. Kushima, B. Yildiz "Oxigen ion diffusivity in strained stabilized zirconia: where is the fastest strain?", J. Mater. Chem., 20 4809 – 4819, 2010.

[6] N. H. Perry, T. O. Mason "Grain core and grain boundary electrical/dielectric properties of yttria-doped tetragonal zirconia polycrystal (TZP) nanoceramics", Solid State Ionics, 181 276–284, 2010.

[7] R. Frison, S. Heiroth, J. L. M. Rupp, K. Conder, E. J. Barthazy, E. Müller, M. Horisberger, M. Döbeli, L. J. Gauckler "Crystallization of 8 mol% yttria-stabilized zirconia thin-films deposited by RF-sputtering", Solid State Ionics, 232 29-36, 2013.

[8] T. Falcade, G. Barbosa de Oliveira, D. Pereira Tarragó, V. Caldas de Sousa, C. de Fraga Malfatti "Influence of substrate temperature in the morphology and microstructure of YSZ films obtained on LSM porous substrate via spray pyrolysis", Mater. Sci. Forum, 691 727-728, 2012.

[9] S. T. Palisoc, R. A. Tegio, M. Natividad, S. G. Mendiola, B. Tuason, K. Kaw, Stephen Tadios "Morphology of YSZ thin films on Ag substrate", Int. J. Scientific & Engineering Research, 3 1-5, 2012.

[10] M. V. F. Schlupp, M. Prestat, J. Martynczuk, J. L. M. Rupp, A. Bieberle-Hütter, L. J. Gauckler "Thin film growth of yttria stabilized zirconia by aerosol assisted chemical vapor deposition", J. Power Sources, 202 47-55, 2012.

[11] Y. Wang, L. Liu, H. Liu, X. Song, D. Hong, D. Xu, S. Zhu, Y. Li "Control of self-assembled particles on thin YSZ film deposited by PLD", J. Supercond. Nov. Magn., 25 11-16, 2012.

[12] P. Amézaga-Madrid, A. Hurtado-Macías, W. Antúnez-Flores, F. Estrada-Ortiz, P. Pizá-Ruiz, M. Miki-Yoshida "Synthesis, microstructural, optical and mechanical properties of yttria stabilized zirconia thin films", J. Alloys Compd., 536S S412– S417, 2011.

[13] B. Scherrer, S. Heiroth, R. Hafner, J. Martynczuk, A. Bieberle-Hütter, J. L. M. Rupp, L. J. Gauckler "Crystallization and microstructure of yttria-stabilized-zirconia thin films deposited by spray pyrolysis", Adv. Funct. Mater. 21 3967–3975 (2011).

[14] T. Falcade, D. Pereira Tarragó, C. MeloHalmenschlager, V. Caldas de Sousa, C. Trindade de Oliveira, C. de FragaMalfatti "Elaboration of yttria-stabilized zirconia films on porous substrates", Mater. Sci. Forum, 660-661 707-711 (2010).

[15] F. Smeacetto, M. Salvo, L. ChandruAjitdoss, S. Perero, T. Moskalewicz, S. Boldrini, L. Doubova, M. Ferraris "Yttria-stabilized zirconia thin film electrolyte produced by RF sputtering for solid oxide fuel cell applications", Mat. Lett., 64 2450-2453, 2010.

[16] T. Talebi, M. Haji, B. Raissi, "Effect of sintering temperature on the microstructure, roughness and electrochemical impedance of electrophoretically deposited YSZ electrolyte for SOFCs" Int. J. Hydrogen Energy, 35 9420-9426, 2010.

[17] I. Kosacki, C.M. Rouleau, P.F. Becher, J. Bentley, D.H. Lowndes, "Nanoscale Effects on the Ionic Conductivity in Highly Textured YSZ Thin Films", Solid State Ionics, 176 1319-1324, 2005.

[18] M. F. García-Sánchez, J. Peña, A. Ortiz, G. Santana, J. Fandiño, F. Cruz, J. C. Alonso, "Nanostructured YSZ thin films for solid oxide fuel cells by ultrasonic spray deposition", Solid State Ionics, 179 243-249, 2008.

[19] O. Yamamoto, Y. Arachi, Y. Takeda, N. Imanishi, Y. Mizutani, M. Kawai, Y Nakamura "Electrical conductivity of stabilized zirconia with ytterbia and scandia", Solid State Ionics, 79 137-142, 1995.

[20] V. Vijaya Lakshmi, R. Bauri, S. Paul "Effect of fuel type on microstructure and electrical property of combustion synthesized nanocrystalline scandia stabilized zirconia", Mater. Chem. Phys., 126 741-746, 2011.

[21] B. G. Pollet "The use of ultrasound for the fabrication of fuel cell materials", International J Hydrog. Energy, 35 11986-12004, 2010.

[22] W. Mwakikunga "Progress in ultrasonic spray pyrolysis for condensed matter sciences developed from ultrasonic nebulisation theories since Michael Faraday" Critical Reviews in Solid State Mater. Scien., 39 46-80, 2014.

[23] M. F. García-Sánchez, A. Ortiz, G. Santana, M. Bizarro, F. Cruz Gandarilla, M. A. Aguilar-Frutis, J. C. Alonso "Nanostructured CeO_2 thin films deposited by ultrasonic spray pyrolysis", J. Am. Ceram. Soc, 93 155-160, 2010.

[24] L. Castañeda, A. García-Valenzuela, E. P. Zironi, J. Cañetas-Ortega, M. Terrones, and A. Maldonado, "Formation of Indium-Doped Zinc Oxide Thin Films Using Chemical Spray Techniques: The Importance of Acetic Acid Content in the Aerosol Solution and the Substrate Temperature for Enhancing Electrical Transport," Thin Solid Films, 503, 212-8, 2006.

ISSN: 2319-5967
ISO 9001:2008 Certified
International Journal of Engineering Science and Innovative Technology (IJESIT)
Volume 3, Issue 3, May 2014

[25] M. Hartmanová, F. Kubel, V. Buršíková, E. E. Lomonova, J. P. Holgado, V. Navrátil, K. Navrátil, F. Kundracik "Phase composition-dependent physical and mechanical properties of $Yb_xZr_{1-x}O_{2-x/2}$ solid solutions", J. Phys. Chem. Solids, 69 805-814, 2008.

[26] M. Hartmanová, E. E. Lomonova,F. Kubel, J. Schneider, V. Buršíková, M. Jergal, V. Navrátil, F. Kundracik "Relationship between effective ionic radii, structure and electro-mechanical properties of zirconia stabilized with rare earth oxides M_2O_3 (M = Yb, Y, Sm)", J. Mater. Sci., 44 234-243, 2009.

[27] M. Jouanne, J.F. Morhange, M.A. Kanehisa, E. Haro-Poniatowski, G.A. Fuentes, E. Torres, E. Hernández-Tellez, "Structural transformations in nanosized zirconium oxide", Phys. Rev. B 64 155404, 2001.

[28] A. Hartridge, M. Ghanashyam Krishna and A. K. Bhattacharya "Optical properties of nanocrystalline ytterbia doped zirconia thin films", Int. J. Mod Phys, 14 1017-1024, 2000.

[29] M. Harris, H.A. Macleod, S. Ogura, E. Pelletier, B. Vidal, "The relationship between optical inhomogeneity and film structure", Thin Solid Films, 57 173–178, 1979.

[30] M. F. García Sánchez, J.C. M´Peko, A.R. Ruiz Salvador, F. Fernández Gutierrez, G. Rodríguez Gattorno, A. Delgado, Y. Echevarría Inastrilla "An elementary picture of the dielectric spectroscopy in solids: Physical Basis", J. Chem. Educ., 80, [9] 1062-1074, 2003.

[31] J.-C. M'Peko, J. S. C. Francis, R. Raj "Impedance spectroscopy and dielectric properties of flash versus conventionally sintered yttria-doped zirconia electroceramics viewed at the microstructural level", J. Am. Ceram. Soc., 96 3760-3767, 2013.

[32] M.-F. García-Sánchez, N. Fernández, M.-L. Martínez-Sarrión, L. Mestres, G. Santana, A. R. Ruiz-Salvador "Chemical insertion in the perovskite solid solutions $Pr_{0.5+x-y}Li_{0.5-3x}Bi_{y-2x}TiO_3$: implications on the electrical properties", Mater. Sci. Eng. B, 177 563-569, 2012.

[33] N. Fernández, P. Escribano, E. Cordoncillo, H. Beltrán, M.F. García-Sánchez, I.C. Romero-Ibarra, N. Masó. "Crystal structure and electrical properties of $La_{0.45}Ce_{0.1}Li_{0.27}TiO_3$ synthesized by sol-gel technique", New J. Glass Ceram., 2 59-64, 2012.

[34] S. Dikmen, P. Shuk, M. GreenbIatt, "Hydrothermal synthesis and properties of $Ce_{1-x}LaxO_{2-\delta}$ solid solutions", Solid State Ionics, 126, [1] 89-95, 1999.